Am J Physiol Heart Circ Physiol 300: H879–H891, 2011.
First published January 14, 2011; doi:10.1152/ajpheart.00433.2010.

Blood flow dynamics of one cardiac cycle and relationship to mechanotransduction and trabeculation during heart looping

Barbara Garita,[1,2] Michael W. Jenkins,[3] Mingda Han,[1] Chao Zhou,[4] Michael VanAuker,[2] Andrew M. Rollins,[3] Michiko Watanabe,[5] J. G. Fujimoto,[4] and Kersti K. Linask[1]

[1]*Department of Pediatrics, The Children's Research Institute, University of South Florida and All Children's Hospital, St. Petersburg; and* [2]*Department of Chemical Engineering, University of South Florida, Tampa, Florida;* [3]*Department of Biomedical Engineering, Case Western Reserve University, Cleveland, Ohio;* [4]*Department of Electrical Engineering and Computer Science and Research Laboratory of Electronics, Massachusetts Institute of Technology, Cambridge, Massachusetts; and* [5]*Department of Pediatrics, Case Western Reserve University, and Rainbow Babies and Children's Hospital, Cleveland, Ohio*

Submitted 3 May 2010; accepted in final form 5 January 2011

Garita B, Jenkins MW, Han M, Zhou C, VanAuker M, Rollins AM, Watanabe M, Fujimoto JG, Linask KK. Blood flow dynamics of one cardiac cycle and relationship to mechanotransduction and trabeculation during heart looping. *Am J Physiol Heart Circ Physiol* 300: H879–H891, 2011. First published January 14, 2011; doi:10.1152/ajpheart.00433.2010.—Analyses of form-function relationships during heart looping are directly related to technological advances. Recent advances in four-dimensional optical coherence tomography (OCT) permit observations of cardiac dynamics at high-speed acquisition rates and high resolution. Real-time observation of the avian stage 13 looping heart reveals that interactions between the endocardial and myocardial compartments are more complex than previously depicted. Here we applied four-dimensional OCT to elucidate the relationships of the endocardium, myocardium, and cardiac jelly compartments in a single cardiac cycle during looping. Six cardiac levels along the longitudinal heart tube were each analyzed at 15 time points from diastole to systole. Using image analyses, the organization of mechanotransducing molecules, fibronectin, tenascin C, α-tubulin, and nonmuscle myosin II was correlated with specific cardiac regions defined by OCT data. Optical coherence microscopy helped to visualize details of cardiac architectural development in the embryonic mouse heart. Throughout the cardiac cycle, the endocardium was consistently oriented between the midline of the ventral floor of the foregut and the outer curvature of the myocardial wall, with multiple endocardial folds allowing high-volume capacities during filling. The cardiac area fractional shortening is much higher than previously published. The in vivo profile captured by OCT revealed an interaction of the looping heart with the extra-embryonic splanchnopleural membrane providing outside-in information. In summary, the combined dynamic and imaging data show the developing structural capacity to accommodate increasing flow and the mechanotransducing networks that organize to effectively facilitate formation of the trabeculated four-chambered heart.

optical coherence tomography; optical coherence microscopy; endocardium; cardiac jelly; trabeculation; mechanotransduction; cilia

A CRITICAL TRANSITION PERIOD in cardiogenesis relates to the single-chambered, tubular heart undergoing dramatic morphogenesis by looping to become a four-chambered structure with valve leaflets, ventricular trabeculae, and double parallel blood flow. Integration of complex changes associated with looping, starting with the relatively simple heart tube, has been the subject of much study and speculation. The interplay between form and function is hypothesized to be critical for heart morphogenesis (19). Mechanotransduction of the physical forces of blood flow, along with cardiac tube elongation, are suggested to regulate looping to generate the four-chambered heart (27, 30). Using genetic and surgical experiments to compromise cardiovascular function in the zebrafish (19), avian (15, 47, 54), and mouse models (32), investigators have provided evidence supporting the deduction that fluid forces are an important factor in cardiac morphogenesis. What remains unknown is how cardiac function and mechanotransduction systems are coordinated to transduce the changing fluid forces of blood across the cardiac jelly (CJ) compartment to the myocardium.

Using high-frequency ultrasound, the chicken embryo heart has been imaged from stages 9 to 39 (37). Whereas high-frequency ultrasound is excellent at analyzing morphology and function in embryos with four-chambered hearts, the limited resolution becomes an issue for investigating tubular heart development, especially before stage 20. An acoustic medium also is needed to transmit the ultrasound signal, making the process somewhat invasive and not ideal for longitudinal studies. Confocal microscopy has the increased resolution for observing the early stages of development (13), but the penetration depth is lacking and makes confocal incapable of imaging important animal models that develop four-chambered hearts (murine and avian) under physiological conditions. Optical coherence tomography (OCT) has both the resolution (2–15 μm) and imaging depth (1–2 mm) to investigate the tubular avian and murine heart under physiological conditions. The present studies analyzing a single complete cardiac cycle using four-dimensional (4D) OCT directed focus on specific regions of the heart that appear to relate to areas of biophysical significance in the development of form and function during looping. Additionally, optical coherence microscopy (OCM) of the looping murine heart, integrated with immunohistochemical analysis of mechanotransducing molecules, provides new insights as to mechanisms involved in relation to the endocardial, myocardial, and CJ compartments during looping and the development of the trabeculated cytoarchitecture of the four-chambered heart postlooping.

Our analysis of structure-function relationships of a single cardiac cycle is presented in detail. The cardiac cycle is the basic unit of function and, therefore, provides necessary information on cardiac parameters that need to be considered for

Address for reprint requests and other correspondence: K. K. Linask, USF/ACH Children's Research Institute, 140 7th Aveneue South, St. Petersburg, FL 33701 (e-mail: klinask@health.usf.edu).

defining mechanisms of mechanotransduction, i.e., the conversion of physical forces to biochemical cellular directives. The reproducibility of the cardiac cycle among different embryonic hearts for the specific stage analyzed was consistent. The objectives of the described studies were to define, during one cardiac filling (diastole) and ejection of blood (systole), the relationships between the endocardium, myocardium, and CJ in the living embryonic avian heart during mid-looping at Hamburger and Hamilton (HH) stage 13. The results defined several mechanotransducing pathways that coordinate blood flow information with the morphogenetic process, looping.

MATERIALS AND METHODS

OCT and Image Processing

Three quail (*Coturnix coturnix japonica*), embryonic stage 13 hearts, ~48–52 h (2), were monitored in ovo with the ultrahigh-speed 4D OCT system. This stage is comparable to HH stage 13 chick embryos (17) with an intact circulatory system. At the stages reported here, there is little developmental difference between chick and quail embryos: both chick and quail embryos are the same size, and heart development is similar. The quail embryo was used because it has a smaller yolk and is thus easier to monitor underneath the microscope. Using OCT, we recorded data for three quail embryos. Visual comparison of the recorded data demonstrated no differences in the mechanics of the cardiac cycles of each embryo at this stage. Therefore, one cardiac cycle pattern was selected for structural and functional analyses that are described here. The stage 13 avian embryonic heart corresponds to the human heart at ~3–4 wk postconception.

As previously described, the ultrahigh-speed, 4D OCT system in an environmental chamber was used to acquire in vivo data on the embryonic heart (14). A Fourier domain mode locked laser enabled ultrahigh-speed OCT data collection at 235 frames/s (24). By applying an image-based retrospective gating algorithm to the data, the reconstructed image set consisted of 90 volumes (equally spaced in time) spanning a single heartbeat (14). Each three-dimensional (3D) data set comprised the complete C-loop of the embryonic heart. Figure 1 is provided for orientation of the heart analyses, including direction of blood flow, the levels (L1–L6) of the heart analyzed, and depiction of the cardiac compartments. For stage 13 avian hearts that cycle between 2–3 beats/s, one cardiac cycle corresponded to 90 volumes.

We investigated the relationships that exist between the myocardium, endocardium, and CJ at planes perpendicular to the axial direction of the heart tube, and the blood flow path during systole and diastole. Of the 90 volumes of data, we selected 15 for analysis at each level of the heart tube. These 15 volumes were equally spaced in time, 30 ms apart from each other. The temporal resolution of this system ensured that motion artifacts are negligible. The maximum displacement error of the system due to motion artifact would be 10 μm, whereas an OCT system imaging at 8 frames/s can have a motion artifact as high as 250 μm during systole (24). 4D image processing was essential in determining the location of an orthogonal cross section. The 15 volumes were imported into Amira 5.1 (Visage Imaging, San Diego, CA). This image processing program allows the manipulation of the volumetric data, and any plane of view can be selected. Because our interest is focused on defining the changes of the myocardium and endocardium as the blood flows through the heart tube, we acquired cross sections cut perpendicular to the direction of blood flow and analyzed the images.

A midcoronal plane that divided the ventral and dorsal sides was defined first (Fig. 1*B*), and its location was maintained for all volumes. Onto this midcoronal plane, intersecting planes were carefully selected at six different levels along the length of the heart and in correspondence with the blood flow pattern. Levels 1 and 2 (L1 and L2) correspond to cuts made through the outflow and outflow/right ventricle (RV) boundary regions; levels 3, 4, and 5 (L3, L4, and L5) are through the RV and left ventricular regions; and level 6 (L6) is representative of the inflow region (Fig. 1*C*). This procedure resulted in 90 two-dimensional cross sections (15 selected time points during a cardiac cycle at 6 levels) showing the boundaries of the myocardium, endocardium, and CJ areas. The endocardial lumen, the area encompassing the inner myocardial wall, and the area encompassing the outer myocardium were manually segmented for each image, and their areas quantified in pixels using MetaMorph 6.1 (Molecular Devices, Sunnyvale, CA) (Fig. 1*D*). From these segmentations, the area of the CJ was derived by subtracting the endocardial lumen area from the inner myocardial area, and the thickness of the myocardial wall was calculated by subtracting the inner from the outer myocardial areas.

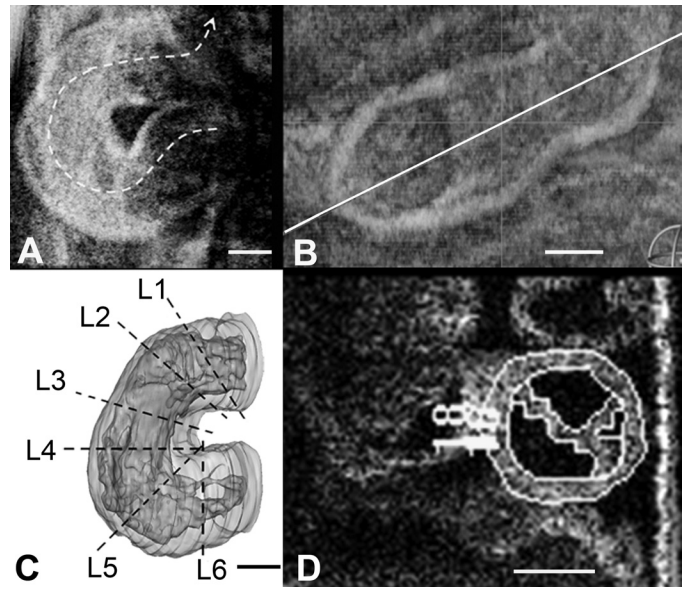

Fig. 1. The embryonic heart as captured in real time and under physiological conditions with optical coherence tomography (OCT). *A*: the dashed white line shows the direction of blood flow on a digitally reconstructed OCT radiograph. *B*: for all 15 volumes analyzed, the placement of the midcoronal plane (white line) was the same. *C*: three-dimensional (3D) reconstruction of Hamburger and Hamilton (HH) stage 13 heart depicts endocardium (Endo) in dark gray, and myocardium (Myo) is transparent in light gray. Six cross-sectional cuts [levels 1–6 (L1–L6)] were defined perpendicular to blood flow. *D*: cross-sectional area measurements of the outer Myo area, endocardial lumen area, and cardiac jelly (CJ) area were performed with MetaMorph 6.1. The outlines are shown in white. Number 18 on figure identifies frame that was used. Magnification bars in all panels = 100 μm.

At the time of OCT monitoring of heart wall motion during looping, the splanchnopleural membrane was noted to be closely apposed to the ventral side of the myocardial wall. As a result, we also analyzed the relationship of the myocardial wall to the extracellular splanchnopleural membrane, as this membrane was suggested to exert a mechanical stress during heart looping and aid in directionality (40), but it was not understood how this may occur. Our high-resolution OCT observations on the relationship are included in Fig. 5.

Area Fractional Shortening Calculation

Area fractional shortening (AFS) is a measurement of the percent change between areas of end relaxation to end contraction in cross sections of the heart wall and endocardial lumen.

OCM

Three wild-type and two heterozygous (NMHC-IIB$^{+/-}$ C57Bl6) mouse embryos on embryonic day (ED) 9.5 were isolated, fixed in 3.5% paraformaldehyde in PBS, rinsed in PBS, and were sent to Dr.

Fujimoto's laboratory at the Massachusetts Institute of Technology (MIT) for OCM imaging. As was earlier reported, the heterozygous embryos showed no morphological differences from the wild type (57). The OCM image of a representative wild-type embryonic heart is shown in Fig. 7 and in supplemental material (fly-through movie; the online version of this article contains supplemental data). A prototype OCM imaging system (1) was developed at MIT and employed for imaging fixed ED 9.5 mouse hearts. OCM is another optical imaging modality based on low-coherence interferometry (23). Unlike confocal microscopy, OCM discriminates reflections in depth by both a confocal and a coherence gate, which increases the signal-to-noise ratio at greater depths (>2-fold increase in depth penetration) and can provide cellular resolution with the lateral resolution approaching 1 μm (21). In this study, for comparison of the avian embryonic heart structure to that of the mammalian mouse embryo at comparable stages, we compared the OCT imaging and analysis of a single heartbeat in the avian embryo with OCM imaging of the mouse embryonic heart. Enhancement of the OCM images of fibrils and cell extensions was done using both Matlab and Amira 5.2.

Immunohistochemistry

The high-resolution immunohistochemical localization protocol for plastic sections that is routinely used in our laboratory has been published (29). Specific extracellular matrix (ECM) and cytoskeletal-related proteins reported to be involved in mechanotransduction were localized in the HH stage 13 to stage 16 hearts during looping. The antibodies used were against the ECM protein fibronectin (FN) (Sigma, St. Louis, MO), ciliar acetylated α-tubulin (58), cytoskeletal α-tubulin (Developmental Studies Hybridoma Bank, Iowa University, IA), tenascin C (TN-C) (IBL, Takasaki-sh, Gunma, Japan), and cytoskeletal nonmuscle myosin heavy chain (NMHC)-IIB (Covance, Emeryville, CA). This is not an exhaustive list, and other molecules could have been considered for analysis, as, for example, fibrillins-1 and -3 (44), fibulin-1 which our laboratory reported on earlier (28), or fibulin-2 (61). To encompass different cellular aspects of mechanotransduction (ECM, cytoskeletal, cilia), the listed subset of molecules was analyzed in this study.

Fluorescence and Confocal Microscopy

Fluorescence microscopy was done using a Nikon Optiphot II microscope. Optical serial sectioning was carried out using a Leica TCS SP II laser scanning confocal microscope at the University of South Florida College of Medicine Imaging Core Facility.

RESULTS

OCT Analysis: Multilevel Cross-sectional Analysis and ECM Relationships

Multilevel cross-sectional analysis of the embryonic heart was used to define tissue relationships of the myocardial, endocardial, and CJ compartments during a single cardiac cycle. The results of the analysis during a complete cardiac cycle are shown in Fig. 2. This figure depicts cross sections shown perpendicular to the blood flow at the above described levels L1–L6 of the heart, passing from anterior to posterior, at 15 time points (t1–t15) during a cardiac cycle, and reading from *left* to *right*. Each level represents 30 ms. There is no precedent to define end-diastole and end-systole for regions of the heart, as analyzed here, because these terms have been used to define only the global relaxation-contraction states of the heart. We describe the patterns of relaxation and contraction throughout the cardiac cycle at a specific level of the heart. Therefore, as the contraction wave was followed along the heart tube, the time when the area of the lumen was largest was defined as the end-relaxation for that specific level of the tube; the time when the area of the lumen was smallest was defined as the end-contraction. These sites of the end-relaxation/contraction states are shaded in red for each level in Fig. 2. For example, at L2 in the RV region, end-relaxation occurred at t2, and end-contraction (underlined) at t8. There were notable cross-sectional area differences between the outflow, ventricular, and inflow regions. In relation to the whole heart, the outflow region (L2) was smallest; the largest regions were the inflow (L6) and the midventricular region (L4). The myocardium was thicker in the inflow region than at any other region in the heart tube. The greatest amount of CJ was in the ventricular region, and the least amount in the outflow region.

Shape analysis in the cross sections revealed that the looping heart myocardium was elliptical in relaxation and more circular during contraction. Throughout one cardiac cycle, the endocardium was more irregularly shaped than any other compartment and displayed multiple folds (Fig. 2), which were especially prominent in the ventricular region. These folds allowed

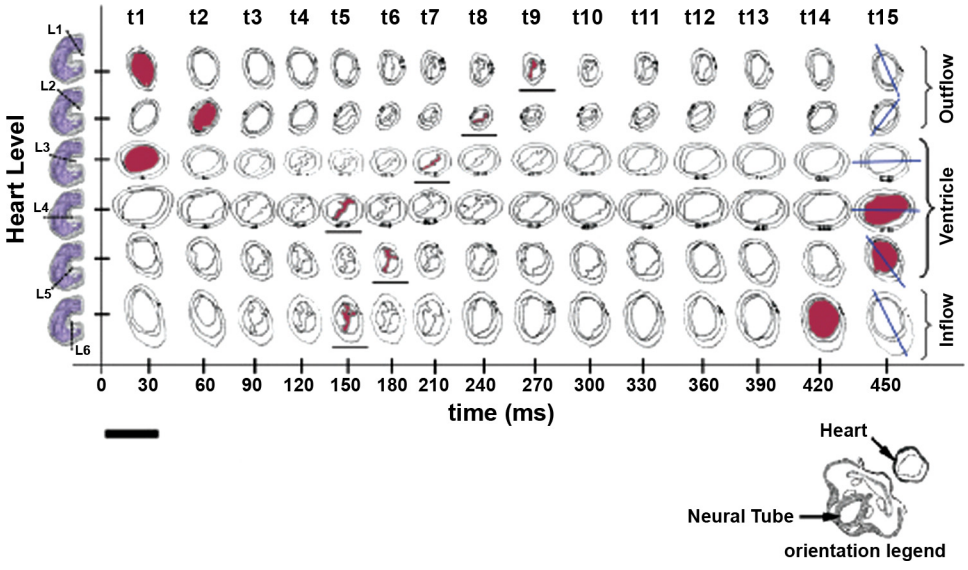

Fig. 2. Cross-sectional cuts are specified at 6 different levels along the length of the heart tube for a HH stage 13 embryonic heart during a cardiac cycle of 450-ms duration. Cuts L1 and L2 are through the outflow region. L3, L4, and L5 cuts are in the ventricular region, and L6 is representative of the inflow region. The red fillings represent end-relaxation, and the underlined tracings indicate end-contraction. All outlines are aligned in a consistent orientation and in accordance with the legend on the *right* corner. At time point 15 (t15) and for all levels, the blue line demonstrates the change in the shape of the heart tube from inflow to outflow during diastole. Orientation of the heart tube relative to the whole embryo is indicated. Magnification bar on *bottom left* of figure = 300 μm.

the cross-sectional area of the lumen to expand from a small area into a relatively large area throughout the cardiac cycle. On average, the inflow (L6) and the midventricular (L4) regions had the largest lumen areas, whereas the outflow (L2) region had the smallest. Figure 2 shows that, during both contraction and relaxation in all cross sections, the endocardium and myocardium remained positioned in this orientation. There were consistent matrix-mediated associations that compartmentalized the CJ to the lateral sides of the heart tube (see Fig. 3). During contraction, specifically in the ventricular region, the endocardium also displayed folds or evaginations (levels L4 and L5 at time t5–t7). For all levels at time period t15, a blue line placed along the long axis of the elliptically shaped heart, in relaxation phase, revealed changes in the axis orientation from inflow to outflow and suggested a twisting motion to the heart.

Immunohistochemical Analysis: ECM-mediated Endocardial Attachment Regions

In all regions of the heart tube as observed above, the endocardium was oriented in the direction of the ventral floor of the foregut and the outermost convex part of the myocardium during the cardiac cycle. This orientation was maintained by ECM-mediated attachments (Fig. 3). To define the composition of the ECM-mediated attachment regions, we used immunolocalization of specific proteins that are reported to be involved in mechanotransduction. The focus was directed to the attachment sites between the myocardium and endocardium that were apparent within the specified six levels of the heart tube within one cardiac cycle. Color encoding in this plate uses green arrows to depict the ventral foregut attachment region, and orange arrows point to the outer curvature. Due to these ECM-mediated embryonic midline attachment sites, the endocardium has a slitlike appearance during contraction of the heart tube.

Sections were cut through a stage 13 (17) embryonic chick heart. Segmentation of the cardiac compartments was done manually using Amira software to create a 3D reconstruction of the looping heart (Fig. 3, *A–C*). The endocardial luminal surface (encoded blue) displayed numerous convolutions (Fig. 3*B*). Figure 3*C* shows surface renderings of the myocardium (pink) and endocardium (blue), along with a cross-section slice. The myocardium is rendered transparent to visualize the endocardium (orange arrows). The specified midline attachment regions (green and orange arrows) were consistently observed. These regions localized proteins, cytoplasmic matrix and ECM, which have been reported to be involved in the transduction of mechanical forces, including FN that localized along the whole length of the heart (Fig. 3, *top* panel, for orientation of Fig. 3*D* at the foregut and Fig. 3*E* at the outer curvature), α-tubulin (Fig. 3, *F* and *G*, at higher magnification), and TN-C (Fig. 3, *H* and *I*, at higher magnification).

FN was highly expressed by the endocardium in both chick and mouse looping hearts (for chick, see Fig. 3*D*; for mouse, Fig. 7*F*, yellow arrows) and at the outer part of the elongated endocardium at the outer curvature (Fig. 3*E*, orange arrows). The FN-mediated attachment at the outer curvature was more apparent in anterior regions of the heart tube during diastole, where the endocardium is more closely associated with the myocardium, than at posterior regions in systole. In cross sections, FN (Fig. 3*E*, green signal, orange arrows) seemingly "tethered" the endocardial endothelial cells to the myocardial wall at the outer curvature region. FN also mediated an attachment of endocardial endothelial cells at the anterior intestinal portal region, as reported previously (28). Multiple FN fibrils consistently extended from the ventral floor of the foregut toward the endocardium, as reported earlier (28). TN-C (see below) also colocalized with FN at the ventral foregut floor attachment region. α-Tubulin localization is shown at low and high magnification, respectively (Fig. 3, *F* and *G*). Evidence

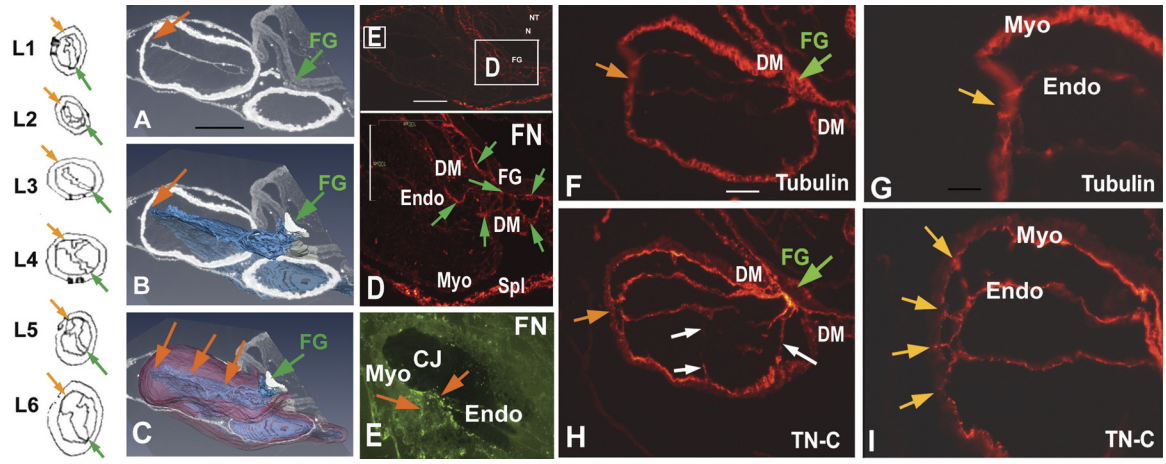

Fig. 3. Mechanotransducing molecules at myocardial-endocardial attachment areas. On *left*, diagrams are tracings of the outlines of the Myo and Endo as captured by OCT at the six levels (L1–L6) of the heart tube from anterior to posterior. The arrows are color-coded defining cardiac areas shown in the figures: orange arrows define outer curvature; green arrows, the ventral midline at floor of the foregut (FG). *A–C*: from serial sections (*A*), a 3D reconstruction of endocardial wall is shown in blue (*B*). *C*: endocardial wall is closely associated with the Myo (color-coded pink) in anterior regions (orange arrows). *D* and *E*: fibronectin (FN) localization. *Top* panel is for orientation, with boxes indicating regions shown in *D* and *E* panels. In *D*, FN (bright red signal) localized at attachment area at the FG, and in *E* (green signal), at the outer curvature where FN tethers the Endo (arrows) to the Myo. *F*: α-tubulin is present throughout Myo. *G*: at the outer curvature region shown at higher magnification, α-tubulin is oriented in direction of strain exerted by the Endo at this site. *H* and *I*: tenascin-C (TN-C) localization in myocardial basal lamina and within the Endo. *I*: 4 TN-C-mediated attachments (arrows) facilitate myocardial-endocardial communication at the outer curvature. NT, neural tube; N, notochord; DM, dorsal mesocardium; Spl, splanchnopleural. Magnifications bars = 180 μm (*A*, *B*, and *C*), 100 μm (*D* and *E*), 76 μm (*F* and *H*), and 38 μm (*G* and *I*).

indicates that both α-tubulin and TN-C are influenced by mechanical stimuli (25, 46). α-Tubulin was present throughout the myocardium. At the outer curvature (orange arrows; Fig. 3, *F* and *G*), the cardiomyocyte microtubules were oriented in the direction of strain that is exerted by the endocardium and where the attachment is mediated by FN and TN-C. In Fig. 3, *H* and *I*, four TN-C-mediated attachments extended to the same outer curvature area, where the myocardium and endocardium interacted and where α-tubulin localized (compare Fig. 3, *F* and *G* with *H* and *I*). Therefore, both FN and TN-C localized to the same attachment areas at the outer curvature of the heart wall and to the ventral foregut in the HH stage 12–16 embryos. These matrix-cytoskeletal-mediated interactions were consistently maintained during looping. Because of these attachment regions, the endocardium takes on the noted slitlike, elongated appearance in end-systole leading into diastole. These attachments also serve to compartmentalize the CJ into left and right sides.

The endocardium displayed convolutions and did not have a smooth central ellipsoid shape as often depicted. We observed these lateral ridges related to fibrils radially connecting the endocardium and myocardium, as also seen in Fig. 3*H* with TN-C lateral fibril localization (white arrows). One part of a lateral attachment was deeper in the CJ and hence out of plane of focus shown here, but apparent in adjacent sections.

OCT Analysis: Wave of Contraction Map

A map of the wave of contraction at the six levels is shown in Fig. 4*A* to demonstrate differences in relative time periods of lumen closure and opening along the length of the heart tube. Systole (defined by black squares) extended for 210 ms in the outflow region (L1 and L2). This time period represents 46% of the total cardiac cycle time. In the inflow region, systole extended for 150 ms, which is 33% of the total cardiac cycle time. These observations indicate that the inflow and outflow regions remain in a state of relative contraction for a considerable amount of time, with the outflow tract period remaining in contraction the longest by 60 ms. The RV and left ventricular regions (L3–L5) show synchronous contractions in lumen area beginning at time t4, indicating a joint contribution to the ejection of blood, as in the four-chambered fetal heart after looping.

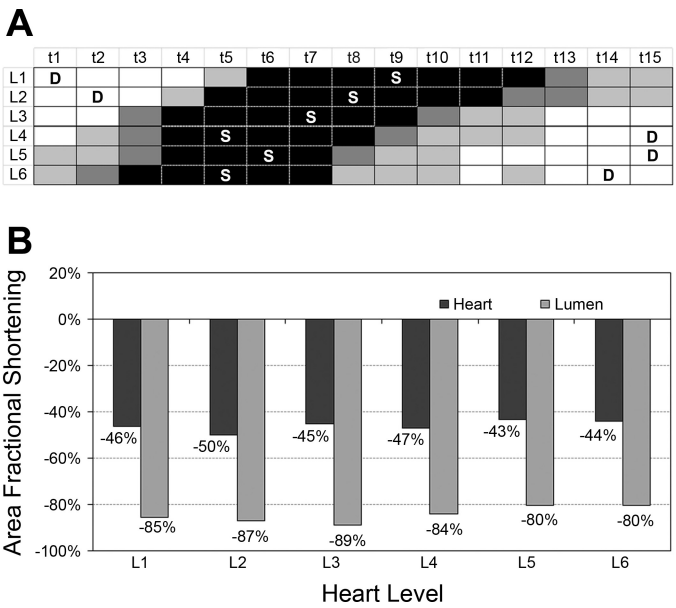

Fig. 4. *A*: peristaltoid map. The S marks the location of end-contraction, and the D of end-relaxation. Black blocks correspond to lumen areas within 25% of end-contraction. Light gray and dark gray blocks correspond to lumen areas that are 50 and 75% of end-contraction, respectively. White corresponds to lumen areas within 25% of end-relaxation. *B*: area fractional shortening (AFS) measurements depict the percent reductions in area from end-relaxation to end-contraction for the heart and Endo lumen at the six heart levels analyzed. The myocardial AFS averages −46 ± 2.4%, and the AFS of the endocardial lumen averages −86 ± 3.5%.

Changes in Area for Myocardium and Endocardium.

The AFS is a measurement of the changes in area from end-diastole to end-systole (Fig. 4*B*). The mean AFS for the myocardial wall and endocardium lumen was −46 ± 2.4 and −86 ± 3.5%, respectively; values are negative because they represent reductions in areas.

OCT of Myocardial Wall Dynamics and Constraints of the Splanchopleural Membrane

The myocardial wall dynamics during contraction and relaxation described above were analyzed also in relation to the extraembryonic splanchnopleural membrane apposed to the myocardial wall (Fig. 5*A*, see arrows). Monocilia have been reported in the myocardium (33, 50). We also identified myocardial monocilia (Fig. 5*B*, white arrows) when using an antibody against acetylated α-tubulin, as used previously to define endocardial monocilia (blue arrow) (58). We show four frames from an OCT movie clip for illustration (Fig. 5, *C–F*), as the heart proceeds from diastole into systole in a peristaltic wave of contraction discussed above. The movie clip is provided in the supplemental material (Splanchno movie). During diastole with endocardial filling with blood, the myocardial wall moved outwards and contacted the splanchnopleural membrane (Sp; red arrows define regions of contact). With continued filling (Fig. 5*C*), the myocardium continued to expand (Fig. 5*D*) and remained associated with the splanchnopleural membrane, as seen over several movie frames (red arrows in Fig. 5, *D* and *E*). The myocardium moved along the membrane for a period of time (in Fig. 5*E* remaining in contact between the red arrows). During myocardial wall contraction (Fig. 5*F*), it pulled away from the extraembryonic membrane. The cycle repeated.

OCT Analysis: Behavior of CJ in One Cardiac Cycle

The behavior of the CJ was analyzed for a single cardiac cycle and at the same previously specified levels along the length of the heart tube. The analyses included changes in CJ cross-sectional area. Each chart in Fig. 6*A* represents levels L1–L6 through the heart. As expected, there was a consistent decrease in endocardial lumen cross-sectional area (dashed curve) as the heart cycle progressed from end-relaxation to end-contraction. The behavior of the CJ is defined by the dotted line curve and its overall trend in gray. The data were normalized by subtracting the lumen area by the minimum lumen area, and the result was divided by the maximum lumen area. These graphs demonstrate that there was a progressive increase in the cross-sectional area of the CJ compartment at L1, L2, and L6, up to the time the endocardium had reached

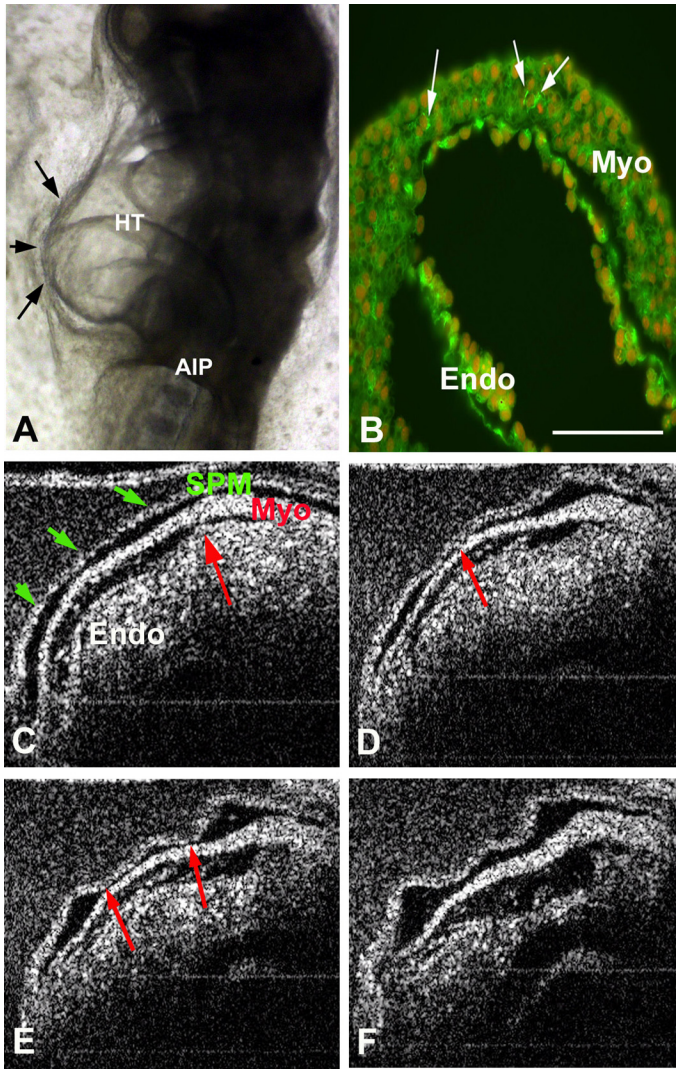

Fig. 5. Looping heart and relationship to Spl membrane (SPM). *A*: looping heart (HT) enclosed in SPM (arrows). *B*: acetylated α-tubulin antibody (bright green signal) localized to monocilia in cardiomyocytes of a stage 17 chick Myo (white arrows). Blue arrows point to a monocilium associated with the endocardial endothelium cells. *C–F*: 4 frames of an OCT movie show the myocardial surface touching the SPM (green arrows) during diastole (*C*; red arrow indicates membrane contact area), then moving further along the membrane (*D* and *E*; red arrows delineate contact region), and then Myo pulls away from membrane during systole (*F*; contraction). Magnification bar in *B* = 76 μm. AIP, anterior intestinal portal.

~50% of its end-contraction cross-sectional area; beyond this point, the CJ cross-sectional area began to decrease in parallel to that of the endocardium. The latter was in contrast to what was observed in L3, L4, and L5 (ventricular regions), where there was little change in the cross-sectional area of the CJ.

Figure 6*B* demonstrates that, at any one moment during the cardiac cycle, the total amount of CJ in the regions of the heart analyzed was relatively constant (mean ± SD, 0.87 ± 0.07). There were, however, small changes in the amount of CJ present at diastole (t1), compared with systole (t7). At diastole, when the endocardial lumen was expanded, there was less CJ (0.79), compared with when the heart was at systole (0.97). There was a nearly linear increase in the CJ as the heart shifted toward systole and a linear decrease as the heart shifted toward diastole.

Immunohistochemical Analysis of the CJ at Looping Stages

During looping, the embryonic heart is compartmentalized into left and right sides by the consistent attachment areas described earlier. At this time, fine fibrillar networks and cell networks are being organized within the CJ. These networks exist within the proteoglycan-rich jelly that undergoes some movement and redistribution described above, as the cells maintain attachments with the myocardium and endocardium. These mechanosensing networks, as a result, undergo cyclical contracting and stretching, as the endocardium and myocardium pass through the contractile cycle.

In addition to TN-C and FN described above, we analyzed the mechanotransducing molecule NMHC-IIB. In the ventricular part of the heart, long thin cell processes were observed in the CJ, as defined by NMHC-II localization (Fig. 7). In Fig. 7*A*, a plastic cross section of a looping avian heart immunostained with NMHC-II antibody and serially cut at 4 μm along its length is shown. Fig. 7*B* depicts NMHC-II-positive fine fibrils or cell extensions color-coded in purple that were apparent within the CJ chiefly in the ventricular region. These same types of attachments and fine fibrils also were observed in a fixed mouse heart on ED 9.5 of gestation, as visualized by OCM and digitally enhanced (Fig. 7*C* and in 7*D* shown at higher magnification). A fly-through movie of OCM images through the mouse heart is provided in the supplemental material. In Fig. 7*E*, an ED 9.5 embryonic mouse heart was immunostained for NMHC-II (red signal), as well as for FN (7F, green signal). NMHC-IIB is expressed by the endocardial cells and by fibrillar-like extensions that connect with the myocardium. NMHC-IIB localized within a fine fibrillar network or cell processes within the CJ. FN also was associated with the endocardium, localized to fibrils extending through the CJ, and mediated attachments between the endocardial evaginations and the myocardial wall (yellow arrows). FN is also expressed by the splanchnopleural membrane. In Fig. 7*F*, the avian endocardial lumen was 3D reconstructed from sections, segmented, and color encoded in blue. The endocardial surface, as described above, was not smooth, but displayed convolutions. The ridges are depicted as darker blue regions that are closely apposed to the myocardial wall. The fine NMHC-II extensions (purple) reconstructed from the sections, when superimposed upon the endocardium, colocalized with the endocardial ridges (yellow arrows in Fig. 7, *F* and *G*). These appear as attachment areas to the myocardial wall. The latter was further analyzed and described below.

CJ, Contractility, and Cardiomyocyte-derived Migrating Cells Leading to Trabeculation

The changes in CJ area, as based on the OCT data, we suggested reflected differential CJ movement and redistribution along the heart tube during the cardiac cycle. Classically, the CJ compartment has been considered acellular. Recent data, however, demonstrate this to be incorrect, because cells begin to move into the CJ during looping with the initiation of trabeculation (41). Thus the cyclical dynamics of each heartbeat imply that any cells directionally migrating into the CJ and that remain associated with the myocardial wall are also subjected to cyclical strain and movement.

To investigate whether cells moving into the CJ remain associated with the myocardial wall, we prepared CJ prepara-

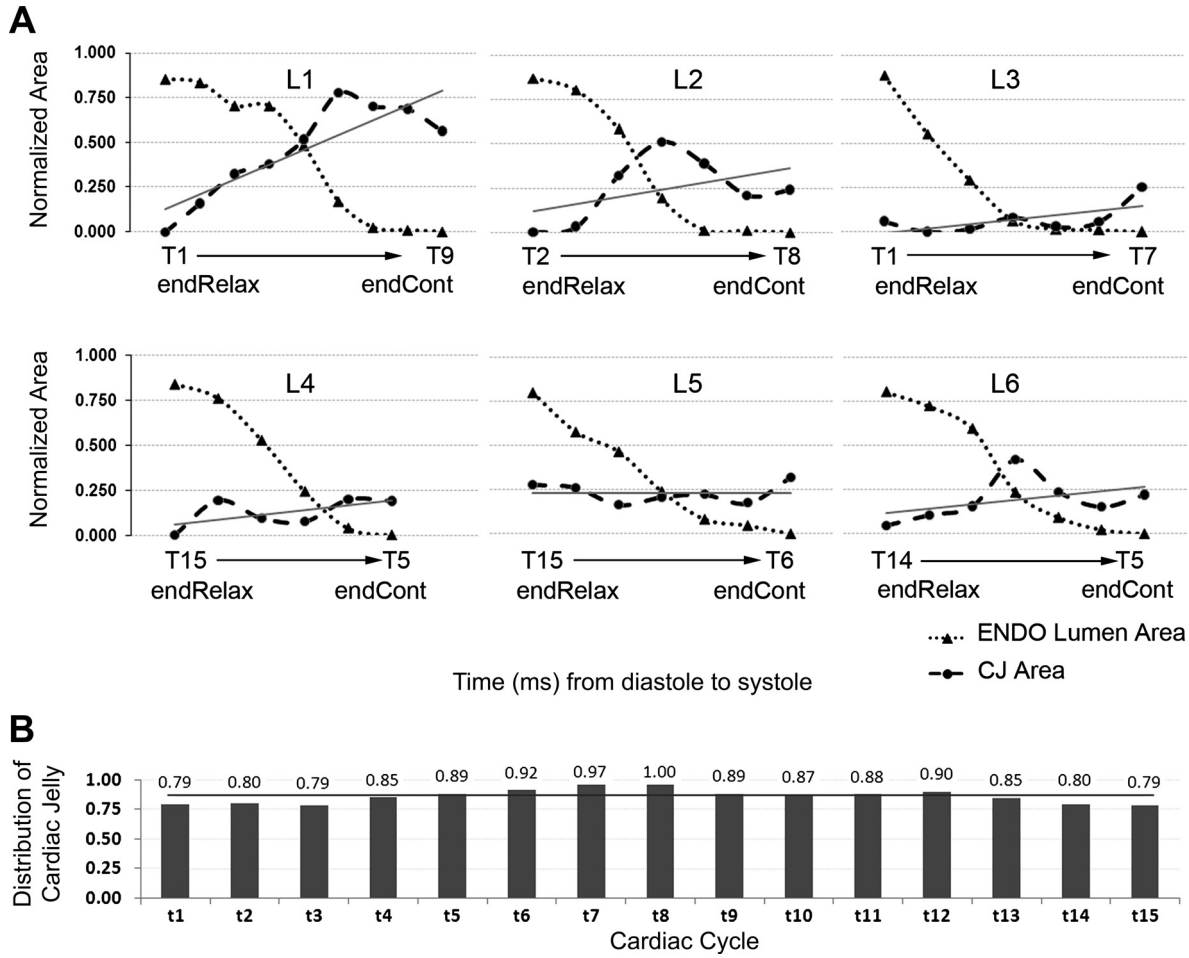

Fig. 6. *A*: multilevel analysis of the behavior of the CJ (dashed line with solid circles) as the Endo area (dotted line with triangles) changes from end-relaxation to end-contraction. L1–L6 on *top* of each curve refer to the heart level, whereas T1, T2, T5, T6, T7, T8, T9, T14, and T15 represent time during the cardiac cycle shown in Fig. 2. endRelax, end-relaxation; endCont, end-contraction. Gray lines represent trend lines for the behavior of the CJ. The data were normalized by subtracting the lumen area by the minimum lumen area, and the result was divided by the maximum lumen area. *B*: normalized quantity of CJ in the heart at the 15 time points during a cardiac cycle analyzed. The solid line is the average (0.87 ± 0.07) for all time points.

tions from HH stage 14–16 looping hearts, using a previously published protocol (39). After isolation, pieces of myocardial fragments and CJ were stained with Coomassie blue for general protein localization (Fig. 8*A*, 8*B* at higher magnification). The myocardial fragments were two cell layers thick, as expected at this developmental stage, in contrast to the single cell layer that is characteristic of the endocardium. At higher magnification, cells and their thin cell processes are visible extending away from the wall (Fig. 8*B*) of the myocardial fragments. To confirm that these were indeed cells, we immunostained the CJ preparations with NMHC-II antibody and with nuclear 4,6-diamidino-2-phenylindole (DAPI) stain (see *inset* in Fig. 8*B*). NMHC-II-expressing cells, a doublet shown here in the *inset* panel, were detectable that also colocalized with DAPI when superimposed. The nucleus of the right-hand cell is easily seen in the *inset*, while most of the cell body is out of plane of focus in this image, but was easily detectable when focusing up and down. The analyses indicated that individual cells directionally migrate from the inner aspect of the myocardial wall into the CJ to initiate trabeculation, but remained associated with myocardial wall cardiomyocytes via long, thin cell processes. These cells also displayed a spatial periodicity. The presence of doublets indicated that these cells generate daughter myocytes that remain interconnected and eventually, after multiple cell divisions, form a network of clonal cells, as was reported by others (41). In Fig. 8*C*, a confocal micrograph of an immunostained whole embryo, the myocardial wall displays NMHC-II cell processes extending from the two-layered myocardium into the CJ.

As based on a temporal study, the relationship between the spatial organization of the migrating "pioneering cells" within the jelly adjacent to the myocardium and trabeculation became evident: in sections of the looping avian heart, initially only a few cells were apparent near the myocardium in the CJ at chick HH stage 12 (Fig. 8*D*). As reported earlier (56), cells also begin to accumulate in the CJ adjacent to the endocardial side, as seen in sections of HH stages 13/14 hearts (Fig. 8*E*). By HH stage 24 (*day 4*), distinct trabeculae were present oriented radially and extending into the CJ from both the myocardial and endocardial compartments (Fig. 8*F*). The orientation of the trabeculae was consistent with the radial arrangement of ECM molecules and NMHC-II extensions, particularly in the ventricular regions that were discernible in the OCM images and in association with the endocardial ridges in the 3D reconstruc-

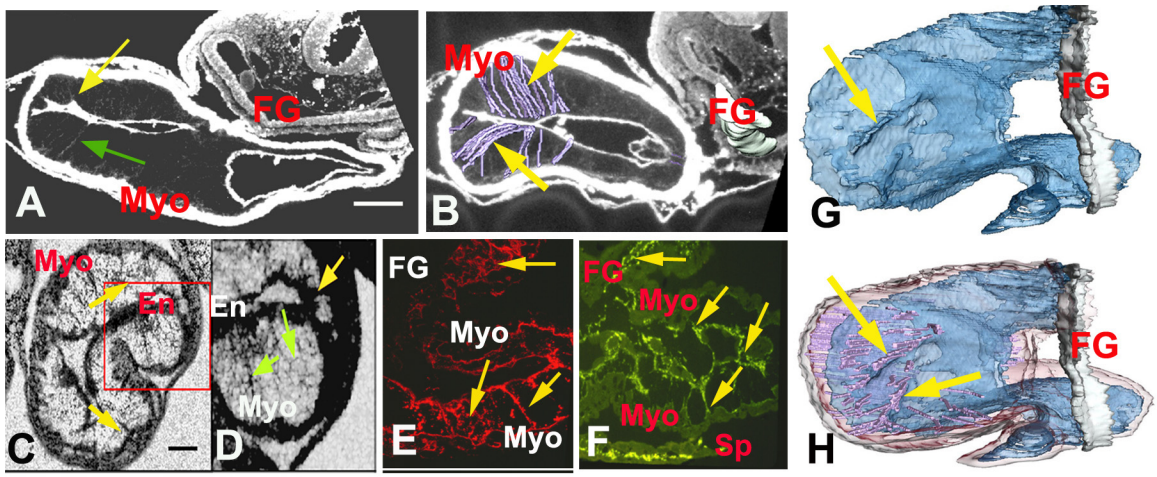

Fig. 7. Fine nonmuscle myosin heavy chain (NMHC)-IIB-expressing cell processes and fibrils extend between Myo and Endo (En). *A* and *B*: adjacent plastic sections through the ventricular region of a looping avian HH stage 13 heart. *A*: cell processes/fibrils (green arrow) extend radially through CJ between the Myo and Endo. Yellow arrow points to the undulating surface of the Endo. In *B*, the cell processes/fibrils were color-coded in purple. *C* and *D*: optical coherence microscopy (OCM) images of the looping mouse heart (embryonic *day 9.5*). Endocardial folds are present (yellow arrows), as well as a fine fibrillar network in the CJ. Boxed region in *C* is shown at a higher magnification in *D* (green arrows point to cell processes and fibrils in the CJ; yellow arrow, an attachment of the Endo to the Myo). *E*: red Cy-3 immunostaining of NMHC-IIB shows localization to endocardial associations with the myocardial wall and in finer fibrillar-like material in the CJ. *F*: endocardial evaginations associate with the mouse Myo via FN-mediated attachments (yellow arrows; green signal for FN). *G*: 3D reconstruction of the endocardial tube from serial sections as in *A* and *B*. The undulating surface of the avian Endo during looping is evident. The ventral FG wall is encoded in gray and white, here defining the embryonic midline. Dark blue denotes where endocardial wall has evaginated toward the Myo, forming folds and outpocketings. *H*: superimposition of the segmented purple fibrils/processes with the Endo. The cell processes and fibrils colocalized at the endocardial ridges. Magnification bars in *A* and for *B* = 100 μm; in *C* and for *D* = 150 μm. Sp, splanchnopleural membrane.

tion. By HH stage 36 (*day 10*) postlooping, in the four-chambered heart the ventricular region was highly trabeculated (Fig. 8*G*), and the trabeculae remain radially oriented. Direction of strain during the heart wall dynamics is indicated by double-headed arrows in diagrams of a wedge of the heart at the *bottom* of Fig. 8.

DISCUSSION

The avian and mouse embryonic hearts are reliable models of the human heart at early stages of development. Imaging of the beating, looping, avian heart by 4D OCT provided insights into the dynamic interrelationships that exist between the three cardiac compartments at HH stage 13, i.e., between the myocardium, CJ, and endocardium. By analyzing the behavior of these compartments perpendicular to the flow of blood, we found evidence that cardiac function was coordinated closely with the assembly of an organizational cellular-ECM network that appears vital for looping and for transduction of biophysical forces to initiate cellular biochemical signaling pathways for organogenesis. A structural-functional relationship in cardiac growth and remodeling has been described as based on conotruncal measurements (26) and use of venous clips (52). We provide new data on how the biophysical changes can be mechanotransduced to affect morphogenesis.

Cardiac Compartment Changes and Relationships

The endocardium displays consistent attachment points during looping. The shape of the endocardium along the length of the tube is more complex than previously detected (34). As shown in Fig. 2 (e.g., L4, t6), the endocardium forms folds that extend toward the myocardium and attach to it at specific regions. We suggest these endocardial folds allow for the endocardial cavity to expand and to accommodate the increasing volumes of blood that enter the heart during looping (20), while also providing structural stability to the endocardial tube via the FN- and TN-C-mediated attachments that form between the endocardium, the myocardium, and the midline of the ventral floor of the foregut. Without the structural stability provided through attachments to the myocardium, the endocardium tube could shift back and forth, preventing regularity in the cardiac cycle.

Other investigators observing the shape of the endocardium during the cardiac cycle at a similar developmental stage have concluded that, during end-systole, the endocardium is slit-shaped, and, during end-diastole, it is elliptical (12, 34). In general, we agree with these conclusions. We extend the previous observations, however, with identification of fibrous attachments that extend from the endocardial wall to the myocardium, providing a complex shape to the endocardium. Presumably, the endocardium requires these attachments to stabilize lumen orientation and to compartmentalize the CJ laterally. We also suggest that these attachments provide a form of structural communication, or mechano-communication, between the myocardium and endocardium at specific sites that is critical for the developmental progression of the early beating heart and for trabeculation (30, 35). The attachments at the midline of the ventral floor of the foregut and at the outermost region of the convex part of the heart are consistently maintained. The endocardial folds and attachments with the myocardium remain consistent, but patterning of folds along the heart tube appears to vary among different embryos. The difference may reflect developmental age differences among embryos and in the amount of blood flow. The precise developmental timing of analysis from embryo to embryo is not possible.

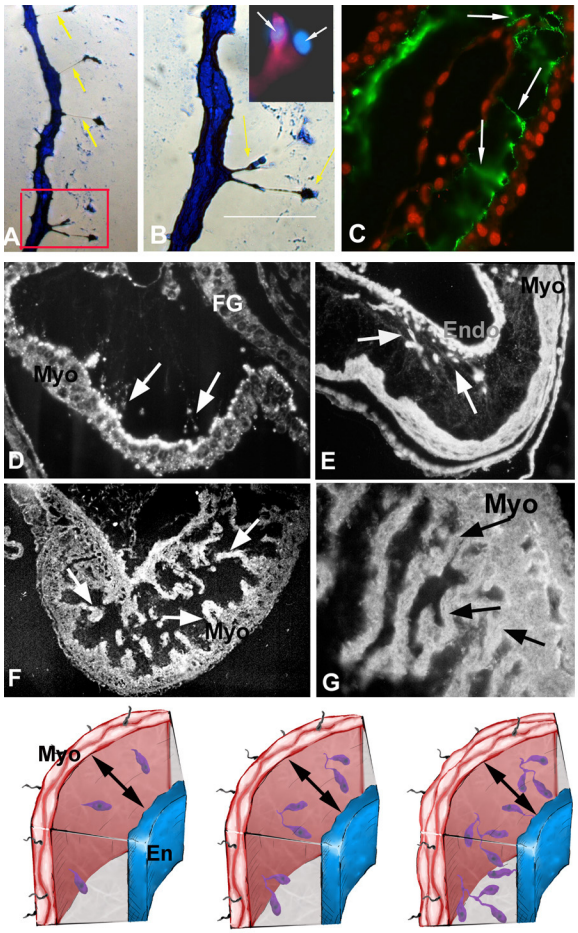

Fig. 8. Initiation of trabeculation is associated with looping stages and NMHC-II expressing cells. *A* and *B*: isolated myocardial fragments of HH stage 13/14 hearts show a two-layered Myo with cells extending from the wall, but remaining attached (yellow arrows). The cells in red boxed-in region in *A* are shown at higher magnification in *B*. Superimposed images of immunolocalization of NMHC-II with nuclear 4,6-diamidino-2-phenylindole staining (arrows pointing to such a doublet of cells in *inset*) demonstrate that these are cell structures within the CJ. *C*: confocal micrograph of a chick looping heart at stage 13 immunostained for NMHC-II shows fine cell extensions in CJ extending from the Myo basal lamina toward the Endo. *D–G*: a cellular organization characteristic of trabeculation becomes apparent between HH stages 12 and 16. *D*: a cell is present in the CJ near Myo at HH stage 13 with NMHC-IIB in CJ beginning to organize (arrows). *E*: similarly, cells are observed in the CJ near Endo at HH stages 13/14. *F*: by *day 4* postlooping, distinct trabeculae (arrows) are apparent, showing similar periodicity as "pioneer" cells in *A*. *G*: by *day 10*, the ventricular region is highly trabeculated (arrows), maintaining the spacing that was evident earlier. *Bottom* row: diagrams of a wedge through the ventricular region of a tubular heart shown at different stages to illustrate our hypothesis: the initial pioneer cells lead to cellular clones of cells, forming a network in the CJ that postlooping has formed the trabeculae. The double-headed arrow depicts the expected direction of strain within the CJ and cellular networks during systole and diastole. Magnification bar in *A* and *C* = 100 μm; *B* = 33 μm.

The elliptical shape of the heart and chamber orientation. At end-diastole, the myocardium has an elliptical shape, and at end-systole it has more of a circular shape. This finding conflicts with previous reports (34), in which the heart was depicted as circular at end-diastole and elliptical at end-systole. These differences in interpretation most likely are due to differences in imaging resolution and/or to the fact that we analyzed cross-sectional cuts perpendicular to the direction of flow.

In observations of OCT movies and data from other hearts, as well as the detailed analyses shown in this report, we note that the long axis of the elliptically shaped heart during diastole is not oriented consistently in the same direction along the length of the tube, but rather the direction of the long axis changes along the length of the tube (Fig. 2, t15). Therefore, we suggest that, as the tube contracts and its shape changes from elliptical to circular, it simulates a wringing motion, which constitutes a more effective physical basis for moving blood out of the heart. This early wringing motion is similar to what has been described for torsion, described for the adult beating heart (7, 48).

Differences in cardiac cross-sectional areas and wall thickness. Different regions or segments of the heart arise sequentially from the heart-forming fields. By stage 13, both the RV and left ventricular regions and the future ventricular inlet (atrioventricular canal) region, as well as part of the outflow associated with the RV, are present (8, 36). The posterior sinoatrial region (inflow) and the anterior conus and truncus of the outflow region continue to develop during looping into stages 14 and 17 (36). In the whole heart, the ventricular region of the heart has the largest cross-sectional area, while the ventricular-outflow boundary region has the smallest. This finding is expected, because the ventricular region is where the maximum amount of blood is maintained before being expulsed through a narrower ventricular-outflow boundary region. In addition, the inflow region has the largest myocardial thickness, possibly because the myocardial contractile strength needs to be strongest in this region to maintain adequate cardiac output. The importance of the inflow region for cardiac output during early heart development was noted in our laboratory's previous studies on the ED 11 mouse heart using Doppler ultrasound (16) and subsequently by others using the chick heart and OCT analysis (24, 53).

Peristaltoid time periods. The timing map shown in Fig. 4*A* illustrates end-systole (S) and end-diastole (D) at different levels along the length of the tube. This figure provides information on the differential time intervals of relative contraction along the length of the tube. The outflow region remains in a state of relative contraction (defined as the lumen area being within 25% of the lumen area at end-systole) for 210 ms, or 46% of the total cardiac cycle time. Of note, 50% of this time period takes place during the beginning of diastole. This extended contraction state allows the ventricular region to fill with blood. In turn, the ventricular region stays longer in a relaxed state, possibly allowing for pressure to increase and resulting in subsequent stronger ejection of blood. At time t4 in Fig. 4*A*, the ventricular region (L3–L5) shows a synchronized contraction that should contribute to the strong ejection of blood. Other investigators have measured very high flow velocities at these same stages (20). These blood flow velocities could be explained by a synchronized contraction of the ventricular regions of the early heart tube. These findings suggest that, at these early stages in development, the heart needs to achieve a high ejection velocity of blood flow, and the stretch-activation response of the myocardium contributes to the performance of a beating heart (59) to achieve this goal. Patten et al. (43) described how the build-up of pressure in the ventricular region leads to high flow velocity. Additionally, the stretching of the cardiomyocytes as pressures build may be necessary for development of the adult myofibrillar organiza-

tion (11, 42, 55). This stretching also may be important for the endocardial endothelial cell regulation of expression of key genes (62). Indeed, the relationship between end-diastolic pressure (or volume) and pressure at end systole, known as the Frank-Starling mechanism in the adult heart, seems to be present already at the 13-somite stage in cardiac development, as was reported also for the later stages of 18, 24, and 29 chick embryos (60).

It would be interesting to correlate our data on time intervals of contraction with the activation sequence revealed by optical mapping data regarding the differences in time spent in contraction via differential duration of action potential. However, little is known about stage 13 in terms of conduction patterns, as investigators analyzing stage 13 have not gotten good signals and indicate only slow conduction of 0.9 cm/s at this stage (9).

AFS. Alexander Barry's conclusions (3) in his often-cited paper on the functional significance of the CJ still holds true. He, however, assumed the shortening of the myocardium was 20% (3). Based on our OCT analysis, we calculated that the AFS for the myocardium is more than twofold higher, i.e., 46%, along the length of the tube. If the myocardium and endocardium tube were in direct contact with each other, they would both have an AFS of 46%. We found that the AFS of the endocardial lumen is ~86% along the entire length of the tube. This discrepancy in AFS between endocardium and myocardium is attributable to the presence of the CJ, and thus it allows for complete closure of the lumen at certain stages during the cardiac cycle, as was suggested also by Barry. In addition, results on modeling of strain patterns on the embryonic heart wall revealed that strain is higher in the inner layer of the early heart tube (6).

Myocardial Wall Dynamics and Constraints of the Splanchnopleural Membrane

The existence of myocardial microcilia was initially reported by Manasek in 1968 (33). Several mechanosensing mutants have been generated in which the mutations affect ciliary biogenesis or mechanosensing pathways. These mutants include the *lrd−/−* mutant with absent node cilia motility, the *Pkd2−/−* mutant with defective ciliary mechanosensation, and the *Kif3a−/−* mutant with complete absence of cilia (50). On the basis of histological descriptive analyses of embryonic hearts immunostained for monocilia in transgenic mouse embryos with these mutations, it was concluded that a subset of cilia, identified as cardiac cilia, is required in heart development that is separate from earlier ciliary function in laterality specification (50). The cited study, however, did not define a role for the presence of cardiac cilia. In a separate analysis, it was shown that, when the splanchnopleural membrane on the ventral surface of the embryo was removed from the chick embryo during looping, torsion was suppressed, a significant increase in myocardial wall stiffness ensued, and looping was affected (40). The source by which the myocardium detects changes in the mechanical force exerted by the splanchnopleural membrane was not defined, but thought to be associated in some manner with the myocardiocyte cytoskeleton.

Our OCT data suggests a mechanism that interconnects the above-cited observations. The myocardial wall during looping touches the splanchnopleural membrane and moves along it for a distance with each heartbeat. As the myocardium rolls along the membrane, the deformation of the myocardial wall along with its microcilia can provide feedback on strains and positional information from the outside in during looping and growth. As looping proceeds over time, the outside-in splanchnopleural membrane strain information would be continuously relayed to the myocardium, positionally slightly changing, as the loop elongates and deepens. As the heart grows, different parts of the myocardium, micron by micron, push against the splanchnopleural membrane with each cardiac cycle. As our data would suggest, when ciliary mechanosensation is altered, abnormal heart development would be observed, as was noted also for the above-described knockout models. The constraint of the extraembryonic membrane aids in maintaining myocardial integrity, the direction of looping, as well as spatially confining the deepening of the loop with cardiac growth, to eventually result in the atria becoming situated cephalad to the ventricles at the end of looping.

OCT Analysis of CJ Changes

As the heart contracts, the curve representing the behavior of the CJ at levels L1, L2, and L6 is distinctive relative to the other levels (Fig. 6*A*). At L2 and L6, the curves show a similar peak in CJ cross-sectional area halfway through the contraction period. This peak signifies that there is an increase in CJ cross-sectional area that accompanies an endocardial decrease in area during systole, but only up to a certain point in systole. After this point, the cross-sectional area of the CJ declines in parallel to that of the endocardial cross-sectional area. This finding suggests that, during contraction, the CJ is recruited into L2 and L6 regions to allow for isovolumetric contraction and to prevent regurgitation. Figure 6*B* shows that the total volume of CJ increases as the cardiac cycle progresses during systole, further suggesting that there is a redistribution of CJ during systole. Both figures, taken together, indicate that there is a greater movement of the CJ in L2 and L6 relative to the other regions we analyzed. Levels L2 and L6 correspond to the valvelike regions of the tubular heart. We hypothesize that these are the regions at which cardiac valves eventually will develop and presage the ultimate fate of these regions as blood-flow regulatory areas. In contrast, L3, L4, and L5 show small changes in CJ cross-sectional area as the endocardial lumen is closing, indicating little change of CJ in the ventricular areas, compared with the inflow and outflow regions.

From projections of successive time-lapse film frames of a live embryonic heart, Patten et al. (43) described the presence of endocardial "mounds" of CJ at specific locations in a 48- to 50-h living embryo where the endocardial lumen is occluded: *1*) between the atrium and the ventricle (atrioventricular canal); and *2*) at the ventricular conus to truncus arteriosus transition area. The previous authors described that CJ mounds "heap up" to obliterate the cardiac lumen and thereby prevent regurgitation of blood. We did not observe heaping of CJ at these locations: instead, closure occurs by actual contraction of the heart (46% AFS). Thus the closure of the endocardium is due to larger changes in myocardial shortening than previously described, and the closure is accompanied by reduction of CJ in these regions (Fig. 6*A*). Together, these structural changes during the cardiac cycle prevent the back flow, regurgitation, of

blood. Confirmatory evidence that heart function is important for valve development is provided by the zebrafish model in which it was shown that, in the homozygous silent heart embryos, which lack a heartbeat due to a mutation of cardiac troponin, the atrioventricular endocardial cushions did not form (4). It would be of interest to analyze whether there is compression of the CJ at the inflow and outflow regions or a squeezing of the CJ into adjacent regions where the heart is continuous with the vasculature.

NMHC-II-Expressing Cells, Mechanotension, and Trabeculation

We report in this study that cells and long myocardial cell processes within the CJ expressing NMHC-II are situated in a radial orientation and were present in both chick and mouse hearts. The OCM data on the mouse embryo confirmed that myocardial-endocardial radial associations exist also in the intact ED 9.5 looping mouse heart.

Our study adds new data for consideration in trabeculation (Fig. 8). Individual cells begin to migrate directionally into the CJ at HH stage 12 (*day 2*) and express NMHC-IIB, a molecule that normally is part of the actomyosin cytoskeleton of the myocardiocyte, has a role in myofibrillogenesis (10) and in cell motility (31), and has an important role in mechanotransduction (5). As the myocardial wall transitions from an epithelium to a trabeculated organ during looping, specific cardiomyocytes, in response to signals from the endocardium, directionally migrate toward the endocardium (51). Confirming our observations, the individual cells were reported to undergo cell divisions, forming a tight cluster or clone of cells that express N-cadherin to maintain their homotypic interactions to eventually give rise to a single or, at most, two trabeculae (41). At the same time as the myocardial side of trabeculation begins, endothelial cells are similarly leaving the endocardium to move into the CJ and have been shown to also play a role in the formation of trabeculae. The migration of both populations orient along the radially aligned matrix molecules that we, using OCM, and others, using scanning electron microscopy, have described in the looping heart (22, 38). During the cardiac cycle, these cells and cellular networks that form continuously experience cyclic strain and stretching (arrow, Fig. 8 diagrams) associated with rhythmic contractions during each cell cycle. Our data, taken together with the cited studies, suggest that these cells undergo myogenesis in response to the cyclical strain of each heartbeat. Cyclical movements of cardiomyocytes can alter gene expression (5, 49, 62) and, with the organization of the ECM, help to shape the characteristic cell organization of the trabeculated ventricular architecture of the four-chambered heart after looping. The importance of hemodynamics in trabeculation is further suggested by a recent report on testing the effects of hemodynamic unloading of the embryonic chick heart: this resulted in disorganized trabeculation and arrested growth (45).

Taken collectively, the cited descriptive studies of transgenic mouse embryo models, as well as avian experimental manipulations, and our present OCT and immunohistochemical data indicate ECM-mediated mechanotransduction of blood flow forces exists in 3D organized mechanosensing networks throughout the CJ associated with the myocardium and endocardium along the length of the looping heart tube. The described ECM and cellular networks form a vital part of transducing physical forces from not only the endocardium to the myocardium, but also external forces of the splanchnopleural membrane to the myocardium, to coordinate development of form with function with each cardiac cycle.

ACKNOWLEDGMENTS

We appreciate the helpful discussions on fetal cardiac function with Dr. Serggio C. Lanata of Brown University, RI. The authors acknowledge Desmond Adler and Robert Huber for technical contributions with the Fourier domain mode locked laser. The authors also acknowledge David Wilson and Madhu Gargesha at Case Western Reserve University for technical contributions to the image processing algorithms used to prepare the data for analysis.

GRANTS

This work was supported by the Suncoast Cardiovascular Research and Education Foundation funded by Helen Harper Brown (K. K. Linask); the Mason Chair (K. K. Linask) from the Foundation of the University of South Florida and All Children's Hospital; and partially funded by the American Heart Association (K. K. Linask). This work was also funded by the US Department of the Army under Award no. W81XWH-05-1-0585 (M. VanAuker). The US Army Medical Research Acquisition Activity (820 Chandler St., Fort Detrick, MD 21702-5014) is the awarding and administering acquisition office. This research is supported in part by National Institutes of Health (NIH) RO1 Awards HL083048 and HL096717 (A. M. Rollins), the Ohio Wright Center of Innovation and Biomedical Research and Technology Transfer award: "The Biomedical Structure, Functional and Molecular Imaging Enterprise", and Interdisciplinary Biomedical Imaging Training Program NIH T32EB007509. This investigation was conducted in a facility constructed with support from Research Facilities Improvement Program Grant no. C06 RR12463-01 from the National Center of Research Resources, NIH. The OCM analysis was supported by NIH R01-CA075289-13 and by Air Force Office of Scientific Research Contract FA9550-07-1-0101 (to J. G. Fujimoto).

DISCLAIMER

Information contained in this article does not necessarily reflect the position or the policy of the government, and no official endorsement is inferred.

DISCLOSURES

J. G. Fujimoto receives royalties from intellectual property licensed by MIT to Carl Zeiss and Lightlabs Imaging.

REFERENCES

1. **Aguirre AD, Hsiung P, Ko TH, Hartl I, Fujimoto JG.** High-resolution optical coherence microscopy for high-speed, in vivo cellular imaging. *Opt Lett* 28: 2064–2066, 2003.
2. **Ainsworth S, Stanley R, Evans D.** Developmental stages of the Japanese quail. *J Anat* 216: 3–15, 2010.
3. **Barry A.** The functional significance of the cardiac jelly in the tubular heart of the chick embryo. *Anat Rec* 102: 289–298, 1948.
4. **Bartman T, Walsh EC, Wen KK, McKane M, Ren J, Alexander J, Rubenstein PA, Stainier DY.** Early myocardial function affects endocardial cushion development in zebrafish. *PLoS Biol* 2: E129, 2004.
5. **Clark K, Langeslag M, Figdor CG, Van Leeuwen FN.** Myosin II and mechanotransduction: a balancing act. *Trends Cell Biol* 17: 178–186, 2007.
6. **Damon BJ, Remond MC, Bigelow MR, Trusk TC, Xie W, Perucchio R, Sedmera D, Denslow S, Thompson RP.** Patterns of muscular strain in the embryonic heart wall. *Dev Dyn* 238: 1535–1546, 2009.
7. **Davis JS, Hassanzadeh S, Winitsky S, Wen H, Aletras A, Epstein ND.** A gradient of myosin regulatory light-chain phosphorylation across the ventricular wall supports cardiac torsion. *Cold Spring Harb Symp Quant Biol* 67: 345–352, 2002.
8. **de la Cruz MV, Sanchez-Gomez C, Palomina MA.** The primitive cardiac regions in the straight tube heart (Stage 9) and their anatomical

expression in the mature heart: an experimental study in the chick embryo. *J Anat* 165: 121–131, 1989.
9. **deJong F, Opthof T, Wilde A, Janse M, Charles R, Lamers W, Moorman A.** Persisting zones of slow impulse conduction in developing chicken hearts. *Circ Res* 71: 240–250, 1992.
10. **Du A, Sanger JM, Linask KK, Sanger JW.** Myofibrillogenesis in the first cardiomyocytes formed from isolated quail precardiac mesoderm. *Dev Biol* 257: 382–394, 2003.
11. **Epstein ND, Davis JS.** Sensing stretch is fundamental. *Cell* 112: 147–150, 2003.
12. **Filas BA, Efimov IR, Taber LA.** Optical coherence tomography as a tool for measuring morphogenetic deformation of the looping heart. *Anat Rec (Hoboken)* 290: 1057–1068, 2007.
13. **Forouhar AS, Liebling M, Hickerson A, Nasiraei-Moghaddam A, Tsai HJ, Hove JR, Fraser SE, Dickinson ME, Gharib M.** The embryonic vertebrate heart tube is a dynamic suction pump. *Science* 312: 751–753, 2006.
14. **Gargesha M, Jenkins M, Wilson D, Rollins AM.** High temporal resolution OCT using image-based retrospective gating. *Opt Express* 17: 10786–10799, 2009.
15. **Groenendijk BC, Hierck BP, Vrolijk J, Baiker M, Pourquie MJ, Gittenberger-de Groot AC, Poelmann RE.** Changes in shear stress-related gene expression after experimentally altered venous return in the chicken embryo. *Circ Res* 96: 1291–1298, 2005.
16. **Gui YH, Linask KK, Khowsathit P, Huhta JC.** Doppler echocardiography of normal and abnormal embryonic mouse heart. *Pediatr Res* 40: 633–642, 1996.
17. **Hamburger V, Hamilton HL.** A series of normal stages in the development of the chick embryo. *J Morphol* 88: 49–92, 1951.
18. **Hogers B, DeRuiter M, Baasten A, Gittenberger-de Groot A, Poelmann R.** Intracardiac blood flow patterns related to the yolk sac circulation of the chick embryo. *Circ Res* 76: 871–877, 1995.
19. **Hove JR, Koster RW, Forouhar AS, Acevedo-Bolton G, Fraser SE, Gharib M.** Intracardiac fluid forces are an essential epigenetic factor for embryonic cardiogenesis. *Nature* 142: 172–177, 2003.
20. **Hu N, Clark EB.** Hemodynamics of the stage 12 to stage 29 chick embryo. *Circ Res* 65: 1665–1670, 1989.
21. **Huang SW, Aguirre AD, Huber RA, Adler DC, Fujimoto JG.** Swept source optical coherence microscopy using a Fourier domain mode-locked laser. *Opt Express* 15: 6210–6217, 2007.
22. **Hurle JM, Icardo JM, Ojeda JL.** Compositional and structural heterogenicity of the cardiac jelly of the chick embryo tubular heart: a TEM, SEM, and histochemical study. *J Embryol Exp Morphol* 56: 211–223, 1980.
23. **Izatt JA, Hee MR, Owen GM, Swanson EA, Fujimoto JG.** Optical coherence microscopy in scattering media. *Opt Lett* 19: 590–592, 1994.
24. **Jenkins MW, Adler DC, Gargesha M, Huber R, Rothenberg F, Belding J, Watanabe M, Wilson DL, Fugimoto JG, Rollins AM.** Ultrahigh-speed optical coherence tomography imaging and visualization of the embryonic avian heart using a buffered Fourier Domain Mode Locked laser. *Opt Express* 15: 6251–6259, 2007.
25. **Jones PL, Chapados R, Baldwin HS, Raff GW, Vitvitsky EV, Spray TL, Gaynor JW.** Altered hemodynamics controls matrix metalloproteinase activity and tenascin-C expression in neonatal pig lung. *Am J Physiol Lung Cell Mol Physiol* 282: L26–L35, 2002.
26. **Keller BB, Hu N, Clark EB.** Correlation of ventricular area, perimeter, and conotruncal diameter with ventricular mass and function in the chick embryo from stages 12 to 24. *Circ Res* 66: 109–114, 1990.
27. **Linask KK.** Regulation of heart morphology: current molecular and cellular perspectives on the coordinated emergence of cardiac form and function. *Birth Defects Res C Embryo Today* 69: 14–24, 2003.
28. **Linask KK, Han M, Cai DH, Brauer PR, Manisastry SM.** Cardiac morphogenesis: matrix metalloproteinase coordination of cellular mechanisms underlying heart tube formation and directionality of heart looping. *Dev Dyn* 233: 739–753, 2005.
29. **Linask KK, Tsuda T.** Application of plastic embedding for sectioning whole-mount immunostained early vertebrate embryos. *Methods Mol Biol* 135: 165–173, 2000.
30. **Linask KK, Vanauker M.** A role for the cytoskeleton in heart looping. *ScientificWorldJournal* 7: 280–298, 2007.
31. **Lo CM, Buxton DB, Chua GC, Dembo M, Adelstein RS, Wang YL.** Nonmuscle myosin IIb is involved in the guidance of fibroblast migration. *Mol Biol Cell* 15: 982–989, 2004.
32. **Lu W, Seeholzer SH, Han M, Arnold AS, Serrano MC, Garita B, Philp NJ, Farthing C, Steele P, Chen J, Linask KK.** Cellular nonmuscle myosins NMHC-IIA and NMHC-IIB and vertebrate heart looping.. *Dev Dyn* 237: 3577–3590, 2008.
33. **Manasek FJ.** A light and electron microscopic study of myocardial development in the early chick embryo. *J Morphol* 125: 329–366, 1968.
34. **Manner J, Thrane L, Norozi K, Yelbuz TM.** High-resolution in vivo imaging of the cross-sectional deformations of contracting embryonic heart loops using optical coherence tomography. *Dev Dyn* 237: 953–961, 2008.
35. **Manner J, Thrane L, Norozi K, Yelbuz TM.** In vivo imaging of the cyclic changes in cross-sectional shape of the ventricular segment of pulsating embryonic chick hearts at stages 14 to 17. A contribution to the understanding of the ontogenesis of cardiac pumping function. *Dev Dyn* 238: 3273–3284, 2009.
36. **Markwald RR, Trusk R, Moreno-Rodriguez R.** Formation and septation of the tubular heart: integrating the dynamics of morphology with emerging molecular concepts. In: *Living Morphogenesis of the Heart*, edited by de la Cruz MV and Markwald RR. Boston, MA: Birkhauser, 1998, p. 43–84.
37. **McQuinn TC, Bratoeva M, Dealmeida A, Redmond M, Thompson RP, Sedmera D.** High-frequency ultrasonographic imaging of avian cardiovascular development. *Dev Dyn* 236: 3503–3513, 2007.
38. **Nakamura A, Manasek F.** Cardiac jelly fibrils: their distribution and organization. In: *Morphogenesis and Malformation of the Cardiovascular System*, edited by Rosenquist G and Bergsma D. New York: Liss, 1978, p. 229–250.
39. **Nakamura A, Manasek FJ.** Experimental studies of the shape and structure of isolated cardiac jelly. *J Embryol Exp Morphol* 43: 167–183, 1978.
40. **Nerukar N, Ramasubramanian A, Taber LA.** Morphogenetic adaptation of the looping embryonic heart to altered mechanical loads. *Dev Dyn* 235: 1822–1829, 2006.
41. **Ong LL, Newrhee K, Mima T, Cohen-Gould L, Mikawa T.** Trabecular myocytes of the embryonic heart require N-cadherin for migratory unit identity. *Dev Biol* 193: 1–9, 1998.
42. **Pan J, Singh US, Takahashi T, Oka Y, Palm-Leis A, Herbelin BS, Baker KM.** PKC mediates cyclic stretch-induced cardiac hypertrophy through Rho family GTPases and mitogen-activated protein kinases in cardiomyocytes. *J Cell Physiol* 202: 536–553, 2005.
43. **Patten B, Kramer T, Barry A.** Valvular action in the embryonic heart by localized apposition of endocardial masses. *Anat Rec* 102: 299–311, 1948.
44. **Rossi A, Weber E, Sacchi G, Maestrini D, Di Cintio F, Gerli R.** Mechanotransduction in lymphatic endothelial cells. *Lymphology* 40: 102–113, 2007.
45. **Sankova B, Machalek J, Sedmera D.** Effects of mechanical loading on early conduction system differentiation in the chick. *Am J Physiol Heart Circ Physiol* 298: H1571–H1576, 2010.
46. **Schroder EA, Tobita K, Tinney JP, Foldes JK, Keller BB.** Microtubule involvement in the adaptation to altered mechanical load in developing chick myocardium. *Circ Res* 91: 353–359, 2002.
47. **Sedmera D, Pexieder T, Rychterova V, Hu N, Clark EB.** Remodeling of chick embryonic ventricular myoarchitecture under experimentally changed loading conditions. *Anat Rec* 254: 238–252, 1999.
48. **Sengupta P, Tajik A, Chandrasekaran K, Khandheria B.** Twist mechanics of the left ventricle: principles and application. *JACC Cardiovasc Imaging* 1: 366–376, 2008.
49. **Sil P, Gupta S, Young D, Sen S.** Regulation of myotrophin gene by pressure overload and stretch. *Mol Cell Biochem* 262: 79–89, 2004.
50. **Slough J, Cooney L, Brueckner M.** Monocilia in the embryonic mouse heart suggest a direct role for cilia in cardiac morphogenesis. *Dev Dyn* 237: 2304–2314, 2008.
51. **Stankunas K, Hang C, Tsun ZY, Chen H, Lee N, Wu J, Shang C, Bayle J, Shou W, Iruela-Arispe M, Chang C.** Endocardial Brg1 represses ADAMTS1 to maintain the microenvironment for myocardial morphogenesis. *Dev Cell* 14: 298–311, 2008.
52. **Stekelenburg-deVos S, Ursem NTC, Hop WCJ, Wladimiroff JW, Gittenberger-De Groot AC, Poelmann RE.** Acutely altered hemodynamics following venous obstruction in the early chick embryo. *J Exp Biol* 206: 1051–1057, 2003.
53. **Taber LA, Zhang J, Perucchio R.** Computational model for the transition from peristaltic to pulsatile flow in the embryonic heart tube. *J Biomech Eng* 129: 441–449, 2007.

54. **Tobita K, Schroder EA, Tinney JP, Garrison JB, Keller BB.** Regional passive ventricular stress-strain relations during development of altered loads in chick embryo. *Am J Physiol Heart Circ Physiol* 282: H2386–H2396, 2002.
55. **Torsoni AS, Marin TM, Velloso LA, Franchini KG.** RhoA/ROCK signaling is critical to FAK activation by cyclic stretch in cardiac myocytes. *Am J Physiol Heart Circ Physiol* 289: H1488–H1496, 2005.
56. **Toyofuku T, Zhang H, Kumanogoh A, Takegahara N, Yabuki M, Harada K, Hori M, Kikutani H.** Guidance of myocardial patterning in cardiac development by Sema6D reverse signalling. *Nat Cell Biol* 6: 1204–1211, 2004.
57. **Tullio AN, Accili D, Ferrans VJ, Yu ZX, Takeda K, Grinberg A, Westphal H, Preston YA, Adelstein RS.** Nonmuscle myosin II-B is required for normal development of the mouse heart. *Proc Natl Acad Sci U S A* 94: 12407–12412, 1997.
58. **Van der Heiden K, Groenendijk BC, Hierck BP, Hogers B, Koerten HK, Mommaas AM, Gittenberger-de Groot AC, Poelmann RE.** Monocilia on chicken embryonic endocardium in low shear stress areas. *Dev Dyn* 235: 19–28, 2006.
59. **Vemuri R, Lankford EB, Poetter K, Hassanzadeh S, Takeda K, Yu ZX, Ferrans VJ, Epstein ND.** The stretch-activation response may be critical to the proper functioning of the mammalian heart. *Proc Natl Acad Sci U S A* 96: 1048–1053, 1999.
60. **Wagman A, Hu N, Clark E.** Effect of changes in circulating blood volume on cardiac output and arterial and ventricular blood pressure in the stage 18, 24, and 29 chick embryo. *Circ Res* 67: 187–192, 1990.
61. **Zhang HY, Chu ML, Pan TC, Sasaki T, Timpl R, Ekblom P.** Extracellular matrix protein fibulin-2 is expressed in the embryonic endocardial cushion tissue and is a prominent component of valves in adult heart. *Dev Biol* 167: 18–26, 1995.
62. **Zheng W, Christensen LP, Tomanek RJ.** Stretch induces upregulation of key tyrosine kinase receptors in microvascular endothelial cells. *Am J Physiol Heart Circ Physiol* 287: H2739–H2745, 2004.